A State of Charge Planning Method of a Plug-in Hybrid Electric Truck With Readily Available Navigation Signals

Kaibo Li, Walter Lhomme, Alain Bouscayrol

A state of charge planning method of a plug-in hybrid electric truck with readily available navigation signals

Kaibo Li, Walter Lhomme, Alain Bouscayrol

Abstract: **Optimal energy management for electrified vehicles can be achieved with a prior understanding of the velocity profile, whose prediction accuracy is influenced by the stochastic uncertainty of real driving cycles. This paper proposes a new state of charge planning method for plug-in hybrid electric trucks. The strategy eliminates the need for velocity prediction and relies solely on some readily available signals, such as estimated remaining distance and travel time. This exemption from velocity prediction avoids expensive computational costs, making it possible to use a more affordable processor. To test the strategy, four random driving cycles representing two different vocational uses are selected. The results show that the proposed strategy only increases fuel consumption by 1.3% for unknown urban and long-haul delivery cycles compared to the optimal strategy. Additionally, a sensitivity study reveals the robustness of the method on inaccurate navigation signals. These findings demonstrate that the proposed method is efficient and adaptive, making it suitable for existing truck applications without the need for additional hardware.**

***Keywords*: electric vehicle, plug-in hybrid electric vehicle, energetic macroscopic representation, state of charge planning**

I. INTRODUCTION

Trucks were responsible for 38% of the carbon emissions from road transportation in the European Union in 2017 [1]. Their electrification is essential for the goal of carbon neutrality [2]. Despite the developments in passenger cars, electrified trucks still need considerable R&D efforts, due to cost and technical gaps [3]. To recoup the high cost of the battery, Energy Management Strategy (EMS) is a primary method for reducing fuel consumption [4].

In plug-in hybrid electric vehicles, how to deplete the battery is important since the battery is no longer a pure buffer. Heuristic strategy, such as charge-depleting-charge-sustaining is the simplest real-time strategy. However, it is far from the optimum [5]. Linear SoC planning with a priori knowledge of target distance is another practical strategy. This linear SoC trajectory is not able to optimize the local fuel economy [6]. Additionally, it only exhibits in scenarios where the overall dynamics of the velocity profile are small. For highly variable driving conditions, the control performance will be poor [7]. Better fuel economy can be achieved by optimization-based strategies. For example, the adaptive equivalent fuel consumption minimization strategy [8] is based on the Pontryagin's-minimum principle (PMP). The key is to define an equivalent factor (or the co-state λ for PMP), which can be pre-defined if the driving cycle is known in advance. This is only possible for fixed routes [9], such as buses or tourism coaches. An obvious drawback is that it cannot adapt to the uncertainties of loads, driving habits, traffics, and environments. In most real-time strategies, the equivalent factor is calculated instantaneously with a controller to track the SoC reference [10-12], it is also called λ - control. In [13], the equivalent factor λ is generated based on an SoC reference by a linear adapter. The maximal/minimal allowed SoC and the average limits of the equivalent factor are required. Nevertheless, these limits are in functions of component average efficiencies, which are sensitive to driving cycles. Therefore, the challenge for an optimization-based strategy is to fastly design an efficient SoC trajectory.

Optimal SoC trajectories rely on the availability of future driving profiles [14], which can be predicted based on a Global Positioning System (GPS), geographic information system [15], or driver's driving habits [16]. Some common algorithms include Markov stochastic processes [17], neural networks [18], or reinforcement learning [19]. Zendegan [20] used the recorded 1750-hour GPS information to estimate the future load of a fuel cell truck. Then a location-based SoC trajectory is defined offline before the start of the trip. This strategy would be more sensitive to uncertainties for ICE-based hybrid vehicles. Xie [21] predefines a long-term reference SoC trajectory linearly in the function of distance, and a short-term SoC reference trajectory is formulated linearly over the predicted horizons by updating the initial SoC. It cannot adapt to changing cycles. To overcome this, Lin [22] proposed a driving pattern adaptive SoC planning method. The driving pattern is divided into three types, and different electricity distribution coefficients (SoC/km) are applied to reformulate the SoC trajectory. This method is sensitive to pattern recognition accuracy. Guo [23] proposed a reinforcement-learning-based SoC planning method at a fixed time step (60s). The reward of reinforcement learning is updated regarding different angular ranges of the possible SoC in the spatial domain. The method makes the final SoC reach its expected value at the end of the cycle. In [24], an adaptive policy optimization is introduced to deal with the SoC long-term dynamics. Different from the reference SoC trajectory, the battery discharge is regarded as an increased probability of SOC shortage, which is estimated to optimize the strategy by a deep neural network. It eliminates the hard restriction by the fixed reference SOC trajectories. This method requires the availability and richness of real-world driving data. Generally, a longer prediction horizon leads to better overall performances. Because more future information will be available for decision making. But a heavier computation burden and a larger memory are required [25]. To overcome this, the optimization problem is linearized and discretized, then the predictive control is converted into a quadratic problem [26]. Li [27] plans the long-term SoC trajectory as a function of total traction energy in different road sections.

Abbreviations

EMR	Energetic macroscopic representation
ICE	Internal combustion engine
PMP	Pontryagin's-Minimum Principle
SoC	State of charge
VECTO	Vehicle energy consumption calculation tool

Nomenclature

A	Coefficient for co-state boundaries
B	Coefficient for co-state boundaries
C	Coefficient for co-state boundaries
D	Coefficient for co-state boundaries
E	Coefficient for co-state boundaries
F	Force
H	Hamiltonian function
J	Inertia of the components
K	Rate of state of charge
M	Mass
P	Power
Q	Capacity of the battery
T	Torque
Ω	Rotational speed
Φ	Cost function
a	Coefficient for optimal control law
b	Coefficient for optimal control law
c	Coefficient engine and electric drive approximation
d	Distance
e	Coefficient
g	Gravity of the earth
k	Gear ratio
m	Mass flow of the internal combustion engine
n	Number axles or wheels
r_{int}	Internal resistance of the battery cell
t	Time
v	Velocity
x	State variable
α	Slope angle
β	Coefficient for rolling coefficient
γ	Gear position
ε	Air drag coefficient
ζ	Coefficient for transmission model
η	Efficiency
λ	Co-sate variable of Pontryagin's-Minimum Principle
σ	Controller
ϖ	Relative axle load of the wheel
ρ	Density
χ	Coefficient for electric drive model

Subscripts

air	Air of the environment
aux	Auxiliary devices
axle	Axle
bat	Battery
base	Baseline
bk	Mechanical brake
bsfc	Brake specific fuel consumption
chassis	Chassis of the truck
ed	Electric drive
ed_e	Electrical component of an electric drive
end	The end of the journey
est	Estimation component
fuel	Fuel of the engine
ice	Internal combustion engine
ISO	International standard
J	Inertia component
lower	Lower limit
mech	Mechanical system
mes	Measurement
_max (or _min)	Maximal or minimal value
ocv	Open circuit voltage
upper	Upper limit
rrc	Rolling resistance coefficient
ref	Reference component
res	Resistance component
remaining	The remaining component
rolling	Rolling resistance
slope	Road slope
tot	Total component
trac	Traction
veh	Vehicle
wh	Wheel

The main challenge is to estimate the total traction energy to define the range of the SoC. This requires cycle information known in advance. Zhou [28] proposed an analytical SoC planning method in energy domain, by dividing the velocity profile into segments with different average velocities and road slopes. Then the SoC reference is planned linearly as a function of traction energy with a constant electricity distribution coefficient in each segment. A high-fidelity forward simulator shows that a near global optimal solution can be obtained. This method is computationally cheap as only simple analytical formulas are used. In [29], a rigorous and in-depth theoretical analysis is conducted, focusing on the optimal charge depletion behaviors in the energy domain. Four aggregated optimal charge depletion behaviors are defined, offering insights into the fundamental comprehension of how these rates perform under distinct driving conditions.

The challenges can be summarized as: (1) Optimal SoC trajectories are achievable only with the preview of driving cycles. (2) Velocity prediction and driving pattern recognition methods are promising but rely on the richness of real-world data, and still cost a lot in computation. (3) The uncertainty of driving habits and traffic makes the velocity preview more challenging [30]. Therefore, an efficient energy management strategy that fully utilizes the existing navigation signals instead of predicting the velocity to approach the optimal solution is worthy of study.

This paper aims to propose an innovative SoC planning method for a plug-in hybrid electric truck only utilizing readily available navigation signals. For this, a parallel hybrid medium-duty truck for good delivery is selected for the case study [31]. An accurate truck model and its control are organized by Energetic Macroscopic Representation (EMR) [32]. The model is derived from the well-established VECTO (Vehicle Energy Consumption calculation TOol) European database [31]. The optimization problem is implemented by an EMR-based forward approach, within the frame of PMP. Instead of using model predictive control, the strategy only uses the readily available signals from a navigation system to plan the quasi-optimal trajectory of the SoC.

The novelty and contributions are summarized as:

(1) A new SoC planning method is proposed, which results in only a 1.3% maximum increase in fuel consumption for unknown urban and long-haul cycles when compared to the optimal strategy, even without predicting the velocity.

(2) The proposed strategy does not depend on velocity prediction or driving pattern recognition, thereby avoiding expensive computational costs and enabling the use of a cheaper microprocessor.

(3) The method can adapt to traveling disturbances as the SoC planning is instantly updated based on readily available navigation signals.

(4) A sensitivity study quantifies the influence of estimated remaining time error on fuel economy. The results show

that the method remains robust even with inaccurate navigation signals.

The remainder of this paper is organized as follows. Section II deals with the modelling and control of the truck. Section III deduces the EMS with an adaptive SoC planning within the frame of PMP. Section IV presents the comparisons between the developed strategy and the benchmarks, along with a sensitivity study examining the influence of estimated remaining time errors on fuel economy.

II. Modelling ang Control of the Truck

A. Description of the truck

The studied truck is in P2 architecture, where the electric machine is placed at the input of the transmission. P2 is used since it is the preferred topology for trucks [19]. The operating positions of the Internal Combustion Engine (ICE) and the electric drive are tuned by a 6-speed manual transmission (Fig. 1). The auxiliary devices are supplied by the battery. The parameters of the truck (TABLE I) come from VECTO, which is developed by the European Commission to determine the CO_2 emission of trucks [33].

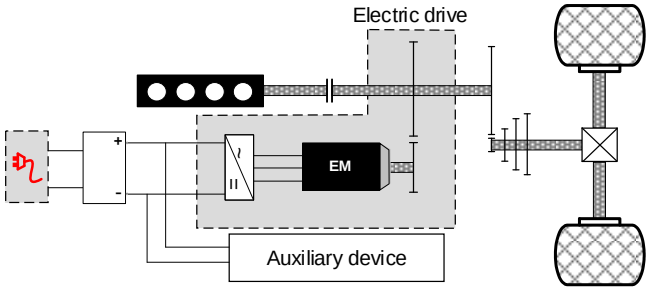

Fig. 1 Configuration of the studied truck with P2 architecture

TABLE I
Parameters of the Studied Truck

Parameters	Values	Parameters	Values
Chassis mass (kg)	4150	AH_{d0}	4.83
Wheel radius (m)	0.4244	Rated load (kg)	2500
Final gear ratio	7.74	Gearbox ratio	2.5
6-speed transmission	[5.375 3.154 2.041 1.365 1 0.791]		

B. Modeling of the truck

The truck is modeled by the equations given in TABLE II. Eq. (1) models the brake-specific fuel consumption $\dot{m}$ of the ICE, it is realized by a 2-D look-up table f_{bsfc} with speed Ω_{ice} and torque T_{ice} as inputs. Eq. (2) refers to battery voltage (u_{bat}) equation, where the internal resistance r_{int} and the open circuit voltage u_{ocv} are functions of SoC. The auxiliary devices is modeled as an equivalent current source i_{aux} with (3) considering a constant power P_{aux}. Eq. (4) describes the parallel connection between the battery, the auxiliary device, and the electric drive. The electric drive current i_{ed} is modeled with (5) by a static model, where the efficiency map η_{ed}, as a function of machine speed Ω_{em} and torque T_{em} is used to describe the losses, χ is to distinguish the direction of power flow. Eq. (6) represents the gearbox with a fixed gear ratio k_{gear} and efficiency η_{gear}. Eq. (7) models the torque Ω_{trac} and speed T_{trac} of ICE and electric drive. Eq. (8) corresponds to the equivalent mechanical transmission of the truck. It includes the 6-speed manual transmission, the final gear, and the equivalent wheel. The equivalent ratio $k_{mech}(\gamma)$ and the efficiency η_{mech} is in function of the gear position γ, ζ is a coefficient. Eq. (9) ,calculates the wheel force F_{wh} by considering the braking force F_{bk}, v_{veh} is the velocity. Eq. (10) refers to the dynamics of the chassis. The moments of inertia of the ICE, electric drive, and wheels (J_{ice}, J_{ed} and J_{wh}) are converted into an equivalent mass, which is a function of the ratio of the transmission $k_{mech}(\gamma)$, torque coupling gearbox k_{gear}, and the radius of the wheel R_{wh}, the number of axles n_{axle}, the number of tires per axle n_{wh}. F_{res} is the resistance. M_{eq} and M_{veh} refer to the equivalent and static mass, M_J is the dynamic mass [34]. Eq. (11) models the resistance force from the environment, which includes the rolling resistance $F_{rolling}$, slope resistance F_{slope}, and air resistance F_{air}, α is the slope angle. The rolling coefficient f_{rrc} depends on the mass of the vehicle. It is modelled as a function of the total mass, the number of axles n_{axle}, the number of tires per axle n_{wh}, relative axle load ϖ, f_{rrc_ISO} and F_{zISO} are the standard rolling coefficient and vertical force, β is a constant coefficient. More details can be found in [35]. The product of front area and air drag ε is a function of velocity.

TABLE II
Modeling Equations of the Studied Truck

$$\dot{m} = f_{bsfc}(\Omega_{ice}, T_{ice}) \quad (1)$$

$$u_{bat} = u_{ocv}(SoC) - i_{bat} r_{int}(SoC) \quad (2)$$

$$i_{aux} = \frac{P_{aux}}{u_{bat}} \quad (3)$$

$$\begin{cases} u_{bat} = common \\ i_{bat} = i_{aux} + i_{ed} \end{cases} \quad (4)$$

$$i_{ed} = \frac{T_{em}\Omega_{em}}{u_{ed}\eta_{ed}^{\chi}(\Omega_{em}, T_{em})} \text{ with } \chi = \begin{cases} 1 & T_{em}\Omega_{em} \geq 0 \\ -1 & T_{em}\Omega_{em} < 0 \end{cases} \quad (5)$$

$$\begin{cases} T_{ed} = k_{gear} T_{em} \eta_{gear}^{\chi} \\ \Omega_{ed} = \dfrac{\Omega_{em}}{k_{gear}} \end{cases} \quad (6)$$

$$\begin{cases} T_{trac} = T_{ed} + T_{ice} \\ \Omega_{trac} = \Omega_{ice} = \Omega_{ed} \end{cases} \quad (7)$$

$$\begin{cases} F_{trac} = T_{tarc} k_{mech}(\gamma) \eta_{mech}^{\zeta}(\gamma) \\ \Omega_{trac} = \dfrac{v_{veh}}{k_{mech}(\gamma)} \end{cases} \quad (8)$$

$$\text{with } \zeta = \begin{cases} 1 & F_{trac} v_{veh} \geq 0 \\ -1 & F_{trac} v_{veh} < 0 \end{cases}$$

$$\begin{cases} F_{wh} = F_{trac} + F_{bk} \\ v_{veh} = common \end{cases} \quad (9)$$

$$M_{eq} \frac{d}{dt} v_{veh} = F_{wh} - F_{res} \quad (10)$$

$$\text{with } \begin{cases} M_{eq} = M_{veh} + M_J \\ M_J = k_{mech}^2(\gamma)\left(J_{ice} + k_{gear}^2 J_{ed}\right) + J_{wh} \frac{n_{wh} n_{axle}}{R_{wh}^2} \end{cases}$$

$$F_{res} = F_{rolling} + F_{slope} + F_{air} \quad (11)$$

$$\text{with } F_{rolling} = M_{veh} g f_{rrc} cos\alpha$$

$$F_{slope} = M_{veh} g sin\alpha$$

$$F_{air} = \frac{1}{2} \rho_{air} \varepsilon(v_{veh}) v_{veh}^2$$

$$f_{rrc} = \sum_{i=1}^{n_{axle}} c_i f_{rrc\_ISO\_i} \left(\frac{\varpi_i M_{veh} g}{n_{wh\_i} F_{zIOS\_i}} \right)^{\beta}$$

Each of the above equations can be translated into Energetic Macroscopic Representation (EMR) elements. EMR is a

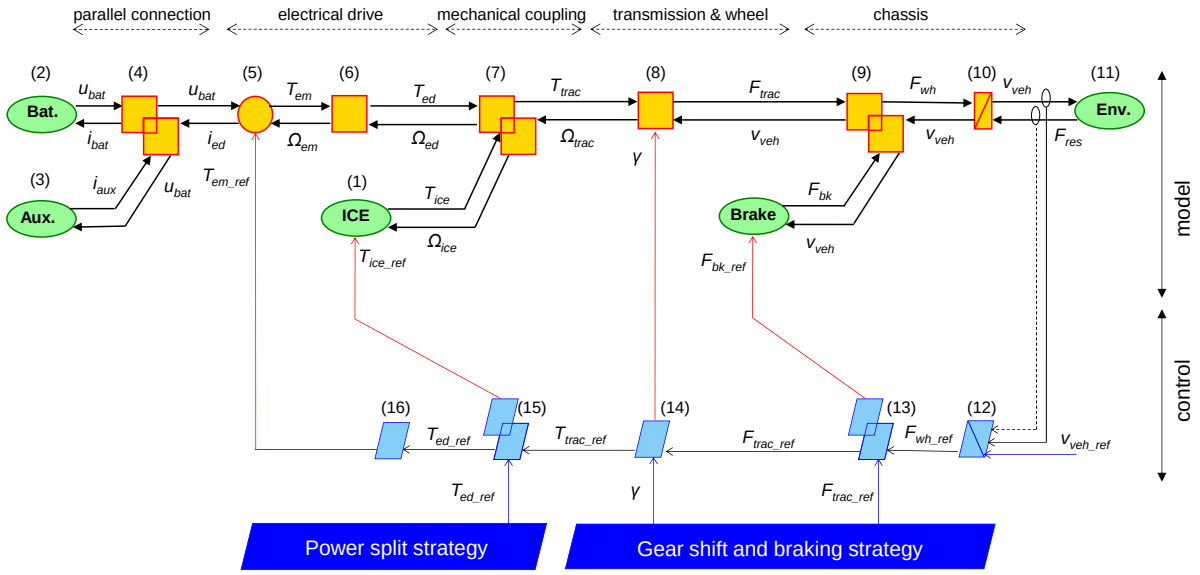

Fig. 2 EMR and control of the studied truck

graphical formalism based on the action-reaction principle to analyze and control systems [32]. It is a multi-physics graphical functional description of energy systems based on physical causality (i.e., integral causality) and cognitive systems. According to the equations above, the EMR of the studied system is given in the upper part of Fig. 2 (with modeling relationships in brackets). All these elements are connected through exchange vectors according to the principle of action and reaction, the product of action and reaction is power. Moreover, the elements are in orange because they exchange powers.

C. *Control of the truck*

From the EMR of the system, the control structure can be deduced step-by-step according to inversion rules [32]. The control of the truck is given by the equations in TABLE III. The inversion of the chassis dynamics (10) is indirectly inverted to obtain the F_{wh_ref} through (12) by using a closed-loop velocity controller σ_{veh}, F_{res_mes} is the measurement or estimation of resistance force. The force coupling relationship (9) is inverted using (13) to calculate the reference of the traction force F_{trac_ref}, by imposing a traction force reference F_{trac_ref}. Eq. (14) is the direct inversion of the mechanical transmission (8), and the gear position γ is given by the gearshift strategy. The mechanical coupling between the ICE and the electric drive (7) is inverted by imposing a torque reference T_{ed_ref} from the power split strategy (15). Finally, the gearbox (6) of the electric drive is inverted using (16).

TABLE III
CONTROL EQUATIONS OF THE STUDIED TRUCK

$$F_{wh\_ref} = \sigma_{veh}\left(v_{veh\_ref} - v_{veh}\right) + F_{res\_mes} \quad (12)$$

$$\begin{cases} F_{bk\_ref} = F_{wh\_ref} - F_{trac\_ref} \\ F_{trac\_ref} = F_{trac\_ref} \end{cases} \quad (13)$$

$$T_{trac\_ref} = \frac{F_{trac\_ref}}{k_{mech}(\gamma)} \quad (14)$$

$$\begin{cases} T_{ice\_ref} = T_{trac\_ref} - T_{ed\_ref} \\ T_{ed\_ref} = T_{ed\_ref} \end{cases} \quad (15)$$

$$T_{em\_ref} = \frac{T_{ed\_ref}}{k_{gear}} \quad (16)$$

The control of the studied truck is shown in the lower part of Fig. 2 (with relationship numbers in brackets). The EMR and its control are in axial symmetry. This scheme is composed of the maximum of control operations and measurements [32]. This structure is so-called the maximum control structure. Continuous lines correspond to the inversion of tuning/control variables while dotted lines are related to the disturbance variables. All control blocks are depicted by blue parallelograms because they handle only information. More details about the modeling and control of an electrified vehicle using EMR could be found in our previous work [36-39].

This truck is hybridized based on a pure ICE-power medium-duty truck, whose model has already been validated in previous work by comparing it with a declared truck from VECTO [40]. And the declared trucks in VECTO are modeled and verified by experiments [41]. Thanks to VECTO, all the components are modeled by the losses or efficiency maps. It ensures a fair simulation at both component and system levels with high-accuracy models.

III. ENERGY MANAGEMENT STRATEGY

As shown in Fig. 2, there are three control variables: the reference of the regenerative braking force F_{trac_ref}, the gear position γ of the manual transmission and the torque reference T_{ed_ref} for power split between the ICE and the electric drive. They are the key elements for energy management.

The gearshift strategy is given by a 2-D look-up table, which is obtained from a support vector machine based on the optimal gear positions of 7 cycles from dynamic programming. A support vector machine is one kind of supervised machine learning algorithm that analyzes data for classification and regression [42]. In practice, the gearshift command is imposed based on velocity and pedal position, the latter can be reflected indirectly by the traction force. So that the inputs of the gearshift strategy are the velocity of the truck v_{veh} and the reference of the traction force F_{trac_ref}, as shown in Fig. 3. The feasible range of the v_{veh}-F_{trac_ref} plane is classified in to 6 different areas, which correspond to the 6 gear positions. More details about constructing classifier can refer to [43].

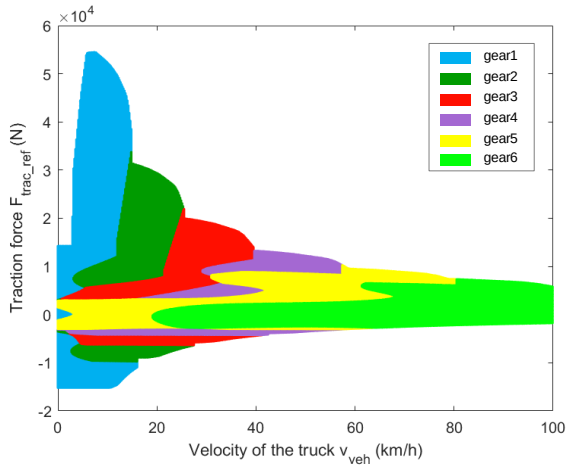

Fig. 3 Gearshift strategy realized by support vector machine

Once the gear position is given, the regenerative braking force F_{tran_ref} during braking can be determined by the following equation:

$$F_{trac\_ref} = \frac{T_{em\_min}(\Omega_{em}) k_{gear} k_{mech}(\gamma)}{\eta_{gear}\eta_{mech}(\gamma)} \tag{17}$$

where T_{em_min} is the limit of the regenerative torque of the electric machine, which is the function of the speed Ω_{em}.

For the power split strategy, the SoC of the battery is selected as the state variable: $x = SoC$, and the torque reference of the electric drive is chosen as the control variable $u = T_{ed\_ref}$. Then the strategy can be stated as follows: finding an optimal control law of $u^* = T^*_{ed\_ref}$ for the truck model to minimize the cost function Φ:

$$\min_u \ \Phi = \int_0^{t_f} \dot{m}\,(u,t) \tag{18}$$

s.t.

$$\begin{cases} T_{ice} \in \left[T_{ice\_min}(\Omega_{ice})\ T_{ice\_max}(\Omega_{ice})\right] \\ T_{ed} \in \left[T_{ed\_min}(\Omega_{ed})\ \ T_{ed\_max}(\Omega_{ed})\right] \\ x_{t_f} \in [SoC_{min} SoC_{max}] \\ x_0 = SoC_0 \end{cases} \tag{19}$$

where T_{ice_min}, T_{ed_min} and T_{ice_max}, T_{ed_max} are the minimal and maximal torques of the ICE and the electric drive; t_f is the length of the cycle; SoC_{min},SoC_{max} and SoC_0 are the lower and upper limits, and the initial value of the SoC.

A. *Pontryagin's-minimum-principle*

In PMP theory, the optimal control law to minimize the cost function (18) can be found in the control law minimizes the Hamiltonian function H:

$$H(x,u,\lambda,t) = \dot{m}(u,\lambda,t) + \lambda\dot{x}(t) \tag{20}$$

where λ is the co-state variable; $\dot{x}$ is the differential of the state variable over time.

The PMP states that if the control law u^* is optimal, the following three necessary conditions must be satisfied:

$$\begin{cases} \dot{x}^* = \frac{\partial}{\partial\lambda} H(x^*,u^*,\lambda^*,t) \\ \dot{\lambda}^* = -\frac{\partial}{\partial x} H(x^*,u^*,\lambda^*,t) \\ H(x^*,u^*,\lambda^*,t) \le H(x^*,u,\lambda^*,t) \end{cases} \tag{21}$$

where the first two conditions refer to the dynamics of the Hamiltonian function; the last condition corresponds to the minimization of the Hamiltonian function.

Eq. (21) in a continuous domain requires differential operations, which nevertheless could be eliminated in discrete time PMP [44]. In this paper, the brake-specific fuel consumption of the ICE ($\dot{m}$) and the electric drive efficiency (η_{ed}) are modeled by look-up tables (see (1) and (5)). Thereby, the ICE and the electric machine need be reformulated.

The brake-specific fuel consumption $\dot{m}$ of the ICE is approximated using a quadratic function of torque T_{ice}:

$$\dot{m} = c_{ice2}(\Omega_{ice})T_{ice}^2 + c_{ice1}(\Omega_{ice})T_{ice} + c_{ice0}(\Omega_{ice}) \tag{22}$$

where c_{ice2}, c_{ice1} and c_{ice0} are the coefficients of the quadratic function. They are in function of the ICE's speed Ω_{ice}.

In the same way, the electric power of the electric machine and its inverter P_{ed_e} is approximated by a quadratic function of torque T_{em}:

$$P_{ed\_e} = c_{em2}(\Omega_{em})T_{em}^2 + c_{em1}(\Omega_{em})T_{em} + c_{em0}(\Omega_{em}) \tag{23}$$

where c_{em2}, c_{em1} and c_{em0} are the coefficients of the quadratic function, they are in function of the machine's speed Ω_{em}.

Then (5) can be reformed as:

$$i_{ed} = \frac{P_{ed\_e}(\Omega_{em},T_{em})}{u_{ed}} \tag{24}$$

The approximations of the ICE and the electric machine are shown in Fig. 4, with several speeds as examples. The original models are well approximated, which proves good accuracy for the reformulation.

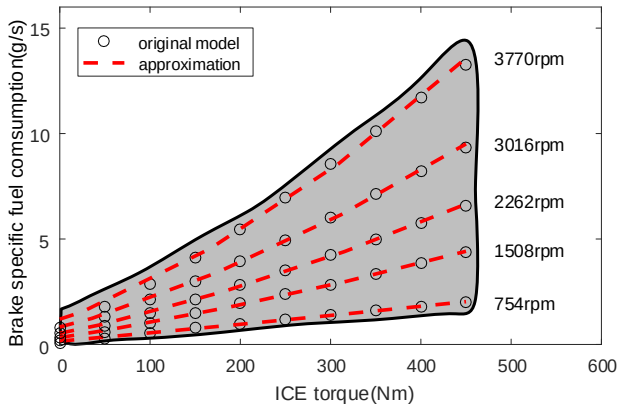

(a) The ICE model

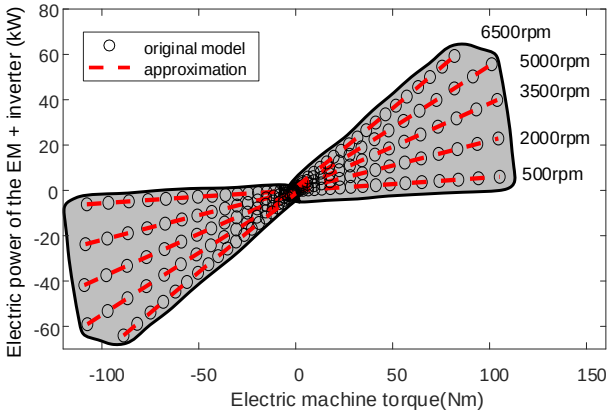

(b) The model of the electric machine + inverter

Fig. 4 Model approximations of the ICE and the electric machine + inverter with several speeds

TABLE IV
INSTANT BOUNDARIES OF THE CO-STATE VARIABLE

	if $C+T_{ed\_min}E>0$	if $C+T_{ed\_min}E<0$	if $C+T_{ed\_min}E=0$
λ_{lower}	$\frac{T_{ed\_min}D-A-B}{C+T_{ed\_min}E}$	λ_{low_est}	λ_{low_est}
λ_{upper}	$\frac{T_{ed\_max}D-A-B}{C+T_{ed\_max}E}$	$min\left(\frac{T_{ed\_max}D-A-B}{C+T_{ed\_max}E},\frac{T_{ed\_min}D-A-B}{C+T_{ed\_min}E}\right)$	$\frac{T_{ed\_max}D-A-B}{C+T_{ed\_max}E}$

When the ICE and the electric machine are reformulated by the above quadratic functions, (21) can be solved. The optimal control law u^* is given by:

$$u^*=\frac{2ab^2c_{ice2}T_{trac\_ref}+ab^2c_{ice1}+\lambda^*bc_{em1}}{2ab^2c_{ice2}-2\lambda^*c_{em2}} \tag{25}$$

with

$$\begin{cases}a=Q_{bat}\sqrt{u_{oc}^2-4P_{bat}r_{int}}\\ b=k_{gear}\eta_{gear}^{sign(P_{ed})}\end{cases} \tag{26}$$

where T_{trac_ref} is the total torque reference of the ICE-electric-drive unit, and it is taken from the control scheme of the forward model; Ω_{em} is taken from the measurement; Q_{bat} is the capacity of the battery. Please note that the studied problem is an optimization with constraints, as shown in (19). The constraints for co-state variable $\lambda^*$is deduced in III.B.

In (25), the optimal control variable u^* is only achievable with an optimal co-state variable λ^*, which is defined by the following equation:

$$\lambda^*=\int_0^{t_f}\lambda^*\left\{\frac{1}{Q_{bat}}\frac{1}{r_{int}}\left(\frac{P_{bat}}{\sqrt{u_{oc}^2-4P_{bat}r_{int}}}-i_{bat}\right)\frac{\partial r_{int}}{\partial x}-\frac{i_{bat}}{\sqrt{u_{oc}^2-4P_{bat}r_{int}}}\frac{\partial u_{oc}}{\partial x}\right\}dt+\lambda_0^* \tag{27}$$

where λ_0^* is the optimal initial value of the co-state variable, which is generally obtained by the shooting method with multiple initial co-states to ensure the same final SoC as the one with dynamic programming [45]. The partial derivation of r_{int} and u_{oc} over x can be defined offline. Nevertheless, the optimal initial co-state is only achievable when the velocity profile is known in advance.

To validate the accuracy of the λ_{opt} strategy (PMP with the optimal λ_0^*), a regional delivery cycle (Fig. 10) is selected. For the benchmark, all the control variables are derived from dynamic programming in a backward approach. The dynamic mass of the truck is also considered. For the λ_{opt} strategy, T_{ed_ref} is calculated using (25) with $\lambda_0^*=-8.823$, the γ is derived from (27) and the regenerative braking force F_{trac_ref} is defined by (17). The comparisons of both strategies are shown in TABLE V.

The λ_{opt} strategy leads to a result close to the optimal one given by dynamic programming. The difference is lower than 1%. This difference can be attributed to several aspects. Firstly, the gearshift command γ of the λ_{opt} strategy is determined using a support vector machine, whereas it is derived from dynamic programming in the benchmark. Secondly, errors are introduced due to the approximations made for the ICE and electric drive in the λ_{opt} strategy. Lastly, the benchmark employs a backward approach, neglecting the truck dynamics in its realization [46].

TABLE V
COMPARISONS BETWEEN PMP AND DYNAMIC PROGRAMMING

	Final SoC	Fuel (L/100km)
λ_{opt} strategy	0.264	11.7
Benchmark	0.265	11.6
Difference (%)	0.4	0.9

B. Instant boundaries of co-state variable

In this subsection, the instant boundaries of the co-state variable will be deduced, which will be used for practical energy management in the following part. Based on (25), the control variable can be rewritten as:

$$T_{ed\_ref}=u=\frac{A+B+\lambda C}{D-\lambda E} \tag{28}$$

with

$$\begin{cases}A=2ab^2c_{ice2}T_{trac\_ref}\\ B=ab^2c_{ice1}>0\\ C=bc_{em1}>0\\ D=2ab^2c_{ice2}>0\\ E=2c_{em2}>0\end{cases} \tag{29}$$

The control variable T_{ed_ref} must satisfy the second constraint in (19):

$$T_{ed\_min}(\Omega_{em})\le T_{ed\_ref}\le T_{ed\_max}(\Omega_{em}) \tag{30}$$

Considering that fact of $D\gg E$, hence $D-\lambda E>0$, we have:

$$\begin{cases}T_{ed\_min}D-A-B\le\lambda\left(C+T_{ed\_min}E\right)\\ \lambda\left(C+T_{ed\_max}E\right)\le T_{ed\_max}D-A-B\end{cases} \tag{31}$$

Since $C+T_{ed\_max}E>0$, while $C+T_{ed\_min}E$ could be positive, negative, or zero. The boundaries of the co-state variable λ are expressed in TABLE IV, where λ_{lower} and λ_{upper} are the instant lower and upper limits of the λ, and λ_{low_est} is the estimated lower boundary. Theoretically, λ_{low_est} is infinitesimal, which corresponds to the case when $C+T_{ed\_min}E=0$. The physical meaning of λ is that it is a factor that converts the dynamic function of the system ($\dot{x}$ in (20)) into an equivalent fuel consumption to be minimized. That means, a lower λ will result in pure ICE-powered mode. Based on the definition of the Hamiltonian function in (20), the value of λ should always be negative. So λ_{low_est} is set as a constant (λ_{low_est} =-50 in this case) to enable the numerical calculation, this value is small enough to disable the electric drive.

C. Dynamical quasi-optimal SoC planning

In braking mode, the regenerative torque of the electric machine should be maximized as much as possible to recover more energy. Hence the co-state variable λ should be set as its upper limit based on its physical meaning:

$$\lambda=\lambda_{upper} \tag{32}$$

In traction mode, the λ is calculated to approach the imposed SoC reference SoC_{ref}. To have an insight into the relationship between SoC and λ, the partial differential of SoC over λ is calculated:

$$\frac{\partial SoC}{\partial \lambda} = \frac{\partial SoC}{\partial P_{bat}} \frac{\partial P_{bat}}{\partial T_{ed\_ref}} \frac{\partial T_{ed\_ref}}{\partial \lambda} = \frac{\partial SoC}{\partial (P_{ed\_e}+P_{aux})} \frac{\partial (P_{ed\_e}+P_{aux})}{\partial T_{ed\_ref}} \frac{\partial T_{ed\_ref}}{\partial \lambda} \quad (33)$$

Considering that the auxiliary power P_{aux} is much smaller than P_{ed_e}, hence P_{aux} is considered as a constant, then (33) is rewritten as:

$$\frac{\partial SoC}{\partial \lambda} = \frac{\partial SoC}{\partial P_{ed\_e}} \frac{\partial P_{ed\_e}}{\partial T_{ed\_ref}} \frac{\partial T_{ed\_ref}}{\partial \lambda} = \frac{\partial SoC}{u_{bat} \partial i_{bat}} \frac{\partial P_{ed\_e}}{\partial T_{ed\_ref}} \frac{\partial T_{ed\_ref}}{\partial \lambda} = -\frac{1}{u_{bat} Q_{bat}} \frac{\partial P_{ed\_e}}{\partial T_{ed\_ref}} \frac{\partial T_{ed\_ref}}{\partial \lambda} \quad (34)$$

The battery capacity Q_{bat} is a constant if the aging process is not considered, and the battery voltage $u_{bat} \approx u_{oc}$ is flat within the allowed SoC range, as shown in Fig. 5.

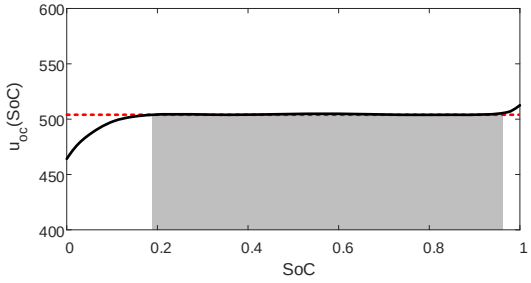

Fig. 5 The battery voltage in the function of SoC

Therefore, the term $\frac{-1}{u_{bat}Q_{bat}}$ in (34) is a constant. Thanks to the quadratic approximation, the electric power $P_{ed\_e}(T_{ed\_ref})$ is approximately linear under different speeds (as shown in Fig. 4), thus the term $\frac{\partial P_{ed\_e}}{\partial T_{ed\_ref}}$ in (34) is also a constant under a specific speed.

Within the feasible range of T_{ed_ref} ($[-150\ 150]$ in this case), $T_{ed\_ref}(\lambda)$, namely (25) is close to being linear. Fig. 6 shows a visualized example of $T_{ed\_ref}(\lambda)$ corresponds to $\Omega_{em} = 400$ rad/s with different torque reference T_{trac_ref}. In this way, the term $\frac{\partial T_{ed\_ref}}{\partial \lambda}$ in (34) is a constant for a certain power demand.

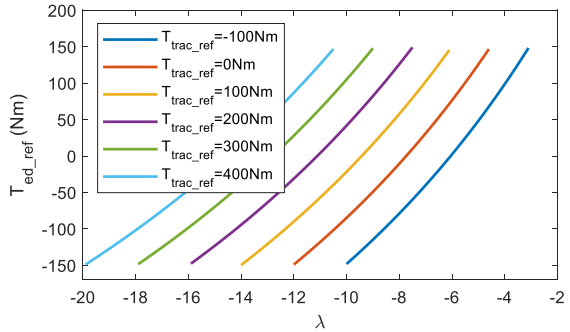

Fig. 6 An example of $T_{ed\_ref}(\lambda)$ with Ω_{em}=400 rad/s

In all, $\frac{\partial SoC}{\partial \lambda}$ is close to a constant for a certain speed and torque demand, and $SoC(\lambda)$ is nearly linear. Then the λ can be given by the following equation based on the relationships of the similar triangles ($\Delta ABC \simeq \Delta AB'C'$) in Fig. 7.

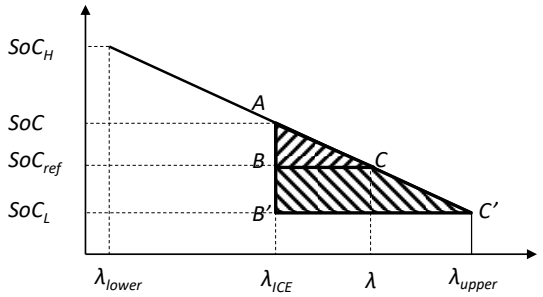

(a) SoC > SoC_{re}

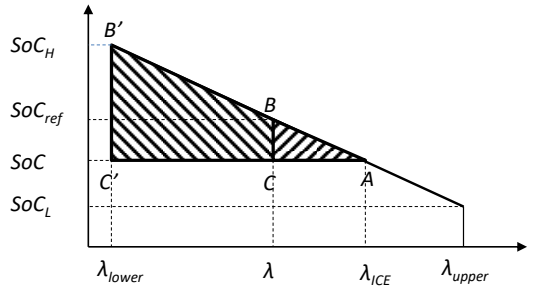

(b) SoC $\leqslant$ SoC_{ref}

Fig. 7 The relationship between SoC and λ

$$\lambda = \begin{cases} \frac{\lambda_{upper}-\lambda_{ICE}}{SoC_L - SoC}(SoC_{ref} - SoC) + \lambda_{ICE} & SoC > SoC_{ref} \\ \frac{\lambda_{ICE}-\lambda_{lower}}{SoC - SoC_H}(SoC_{ref} - SoC) + \lambda_{ICE} & SoC \leq SoC_{ref} \end{cases} \quad (35)$$

where $\lambda_{ICE} = \frac{-A+B}{C}$ is the co-state for pure ICE-powered mode. By utilizing of λ_{ICE} as a baseline, the λ interval used to compute the SoC can be narrowed down. This narrowing of the interval is beneficial in reducing errors that may arise from treating SoC as a linear function of λ. SoC_H and SoC_L are the instant boundaries of SoC, which are defined by:

$$SoC_{H/L} = SoC - \frac{i_{bat\_min/max}}{Q_{bat}} t_s \quad (36)$$

where t_s is the sampling time, $i_{bat\_min/max}$ is the minimal or maximal battery current, which can be calculated from the static model of the electric drive.

The key to this strategy is to define the SoC reference. In the discrete domain, the proposed SoC reference is updated at each sampling time with the following format:

$$SoC_{ref}(k+1) = K(k)\Delta d(k) + SoC(k) \quad (37)$$

where k and $k+1$ represent the present and the next sampling points, $\Delta d(k)$ means the traveled distance between the two adjacent sampling times, $K(k)$ is the instant rate of the SoC over distance.

Regarding the entire remaining distance, we will have the following relationship if the battery is depleted to its minimal SoC at the end of the cycle:

$$\frac{SoC_{min} - SoC(k)}{E_{trac\_remaining}(k)} = \frac{SoC_{min} - SoC(k)}{\overline{F_{wh\_ref}}(k) d_{remaining}(k)} \quad (38)$$

where $E_{trac\_remaining}(k)$ is the demand traction energy at the wheel side for the rest of the cycle, $\overline{F_{wh\_ref}}$ and

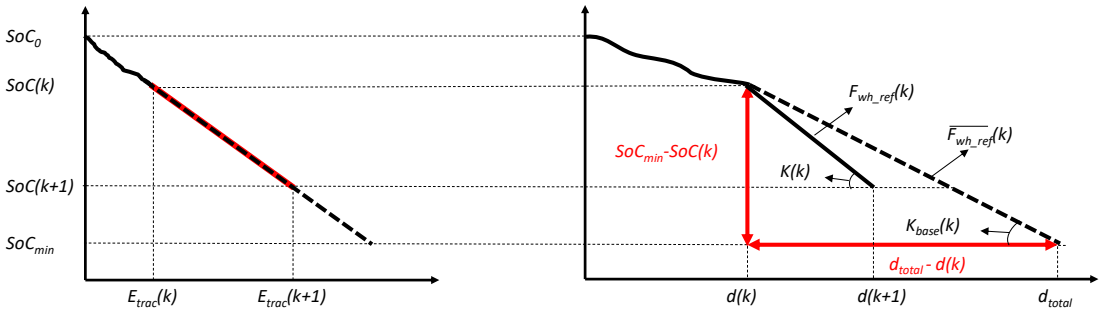

Fig. 8 SoC trajectory transformation between energetic and spatial domains

$d_{remaining}(k) = d_{total} - d(k)$ are the average traction force and the remaining distance of the planned travel. d_{total} is the target travel distance for a planned route, which could be easily obtained from the navigation system.

Regarding a short-horizon period for energy management, the rate of SoC over traction energy can be expressed as:

$$\frac{\Delta SoC(k)}{\Delta E_{trac}(k)} = \frac{\Delta SoC(k)}{F_{wh\_ref}(k)\Delta d(k)} \tag{39}$$

Here it is assumed that the SoC is globally linearly depleted in the function of the traction energy at the wheel side [28, 29]. So that:

$$\frac{\Delta SoC(k)}{F_{wh\_ref}(k)\Delta d(k)} \approx \frac{SoC_{min} - SoC(k)}{\overline{F_{wh\_ref}}(k) d_{remaining}(k)} \tag{40}$$

The instant SoC rate $K(k)$ can be then expressed as:

$$K(k) = \frac{\Delta SoC(k)}{\Delta d(k)} \approx \frac{F_{wh\_ref}(k)}{\overline{F_{wh_{ref}}}(k)} \frac{SoC_{min} - SoC(k)}{d_{remaining}(k)} = \frac{F_{wh\_ref}(k)}{\overline{F_{wh\_ref}}(k)} K_{base}(k) \tag{41}$$

with

$$\overline{F_{wh\_ref}}(k) \approx \overline{F_{slope}}(k) + \overline{F_{rolling}}(k) + \overline{F_{air}}(k) \tag{42}$$

and

$$\begin{cases} \overline{v_{veh}}(k) = \dfrac{d_{remaining}(k)}{t_{est}(k)} \\ \bar{\alpha}(k) \approx \arctan\left(\dfrac{h_{end} - h(k)}{d_{remaining}(k)}\right) \end{cases} \tag{43}$$

$$K_{base}(k) = \frac{SoC_{min} - SoC(k)}{d_{remaining}} \tag{44}$$

where $F_{wh\_ref}(k)$ can be taken from the control of the forward model in Fig. 2. K_{base} is the SoC rate of a virtual baseline. F_{roll}, F_{slope} and F_{air} are the rolling, slope, and air resistances, which are calculated using (11) since the acceleration of the baseline is zero; $\overline{v_{veh}}$ and $\bar{\alpha}$ are the average velocity and road slope of the for the rest of the cycle; t_{est} is the estimated time to complete the remaining distance; $h(k)$ and h_{end} are the road altitudes at the present sampling point and in the end. Parameters of $t_{est}(k)$, $h(k)$ and h_{end} can all be saved from the navigation system. In practical, $F_{wh\_ref}(k)$ is related to the actions on the acceleration pedal.

Based on (37) and (41), the SoC_{ref} can be written as:

$$SoC_{ref}(k+1) = \frac{F_{wh\_ref}(k)}{\overline{F_{wh\_ref}}(k)} \frac{SoC_{min} - SoC(k)}{d_{remaining}} v_{veh}(k) t_s + SoC(k) \tag{45}$$

A visual explanation of the SoC trajectory transformation between energetic and spatial domains is shown in Fig. 8. Even $SoC(E_{trac})$ can be treated linear, the rate of $SoC(d)$ could be different due to different velocities. The above assumption is acceptable due to the following reasons: (1) The plug-in hybrid truck uses as much battery as possible, and the baseline K_{base} can always push the battery to its minimal allowed SoC upon arriving at the destination with a recharging opportunity; (2) Average velocity and road slope are the simplest solutions to realize the K_{base} when only the traveled distance and estimated remaining travel time are available.

The procedure of the strategy implementation is summarized in Fig. 9. The proposed dynamical SoC planning method does not predict the velocity profile (velocity versus time). Instead, it only uses the navigation system to estimate the readily available traveled distance $d(k)$, remaining travel time $t_{est}(k)$ based on current traffic condition and the road altitude $h(k)$. The average velocity $\overline{v_{veh}}$ and slope angle $\bar{\alpha}$ will be estimated firstly, which will be then used to calculate the average traction force $\overline{F_{wh\_ref}}$. The SoC rate is updating dynamically at each sampling time with the help of a baseline K_{base}. The SoC reference will be computed based on F_{wh_ref} and v_{veh} from the

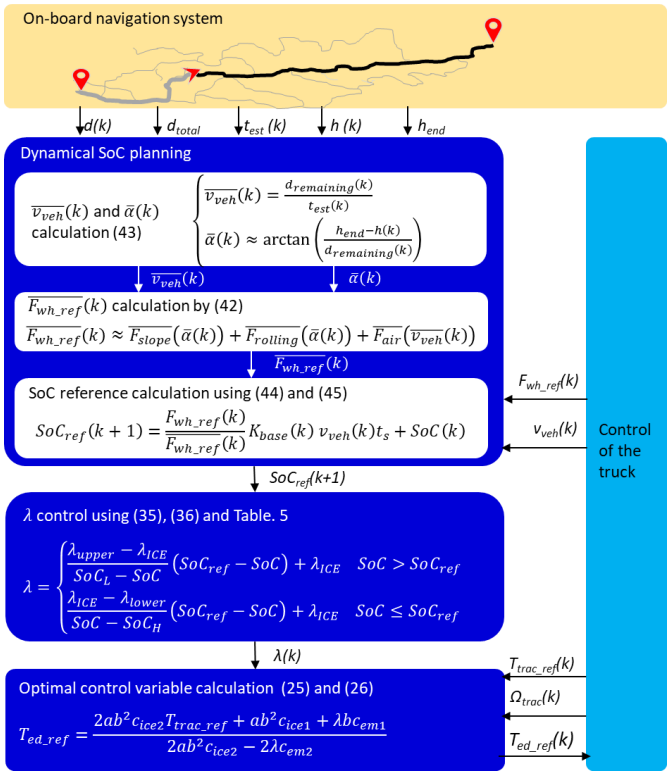

Fig. 9 Summarization of the implementation of the strategy

control structure of the truck. Then the co-state variable $\lambda(k)$ is deduced from $SoC_{ref}(k)$ using (35) and (36). Finally, the optimal control variable $T_{ed\_ref}(k)$ will be deduced based on the T_{trac_ref} and Ω_{trac} The proposed method can take local details into account because the navigation signals will be updated instantly. On the other hand, the required traveled distance, traveling time, and road altitude are much easier to be obtained with the existing hardware.

IV. Simulation and Discussion

To test the strategy, 4 driving cycles for medium-duty trucks are selected (Fig. 10). The selected cycles are composed of 2 types to validate the robustness of the strategy for different vocational uses. The first type refers to urban delivery (heavy urban and urban), where there are many transient states. The second type corresponds to long-distance and high-speed transportation (long haul and regional delivery), where the velocity is high and there are9 fewer transient states. All these cycles are taken from the data set from VECTO.

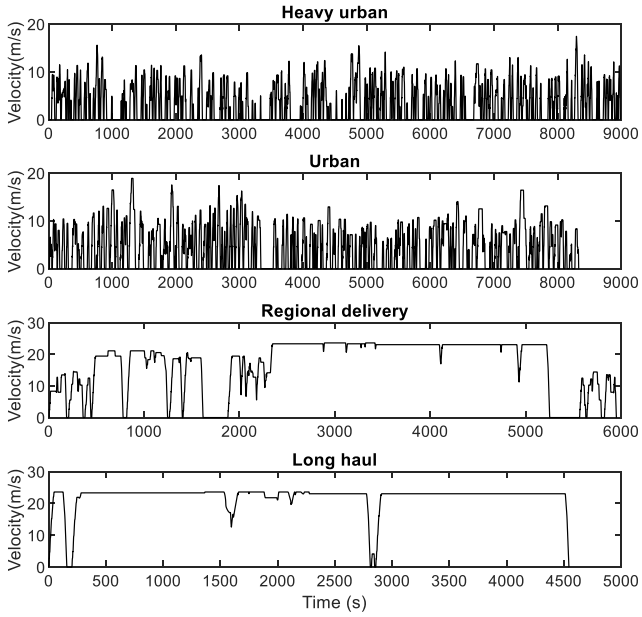

Fig. 10 The selected cycles for the studied truck

A. Results and discussions

Regarding the considered cycles, the λ_{opt} strategy is used as the benchmark for comparisons. To ensure a fair comparison, the proposed SoC planning method is simulated under various driving cycles, and the corresponding final SoCs are recorded. Next, the shooting method is employed to determine the optimal initial co-state for each driving cycle, ensuring that the final SoC matches that of the proposed strategy. This approach guarantees that the same amount of electricity is consumed, leaving fuel consumption as the sole item for comparison. The comparisons in fuel consumption are shown in Fig. 11. It can be seen that compared to the benchmark (λ_{opt} strategy), the proposed strategy only increases energy consumption by a maximal 1.3%. These results are nearly optimal.

Fig. 12 shows the evolution of the SoC and the co-states λ with the proposed strategy and the λ_{opt} strategy under the cycle of regional delivery (repeated 2 times). It can be seen that the two strategies result in different SoC trajectories. Even so, the proposed strategy results in a near-optimal solution. Because the optimal SoC trajectory that leads to minimal fuel consumption is unique, while the SoC trajectory for non-optimal is numerous. Additionally, both strategies reach the same final SoC, namely 0.265 in this case. In the second figure, the gray shadowed area corresponds to the instant feasible area of the co-state. The trajectory of the λ_{opt} has small fluctuations around its initial value, because the capacity of the battery results in a small-time differential of the co-state $\dot{\lambda}$ (referring to the part inside the integral symbol in (27)). Nevertheless, the co-state of the proposed strategy is varying within the feasible range.

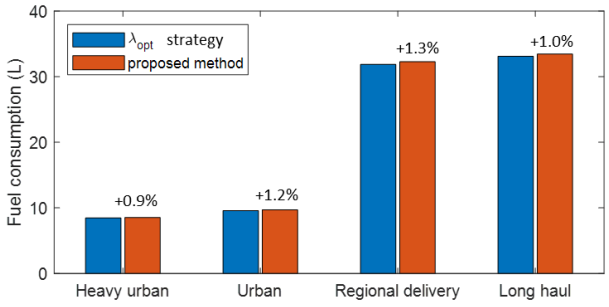

Fig. 11 Comparisons of fuel consumption

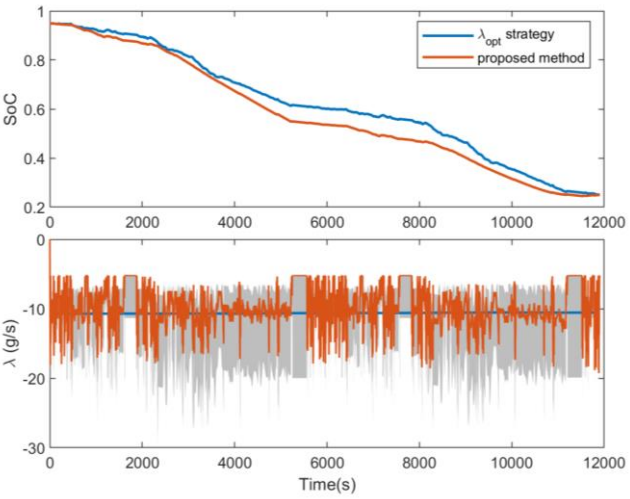

Fig. 12 Comparisons of co-state variables

Regarding the computational efficiency of the strategy, the computational burden was measured to calculate a torque reference. The simulations were performed using MATLAB 2021b on a computer equipped with an Intel(R) Core (TM) i7-10610U CPU @ 1.80GHz 2.30 GHz and 32GB RAM. A fixed step solver with a step size of 1 ms was used for the simulations. The strategy presented in Fig. 8 was calculated 1000 times, and the average computation time is detailed in TABLE VI.

TABLE VI
Execution Time of the Strategy

	Maximal	Minimal	Average
Computation time (ms)	2.4	0.5	1.8

For vehicle-level control, the computation is efficient enough. However, certain model predictive control methods can lead to heavy computational burdens due to factors such as long prediction horizons, complex optimization problems, state estimation, constraints handling, etc. For instance, in the case of battery thermal management, the average computation

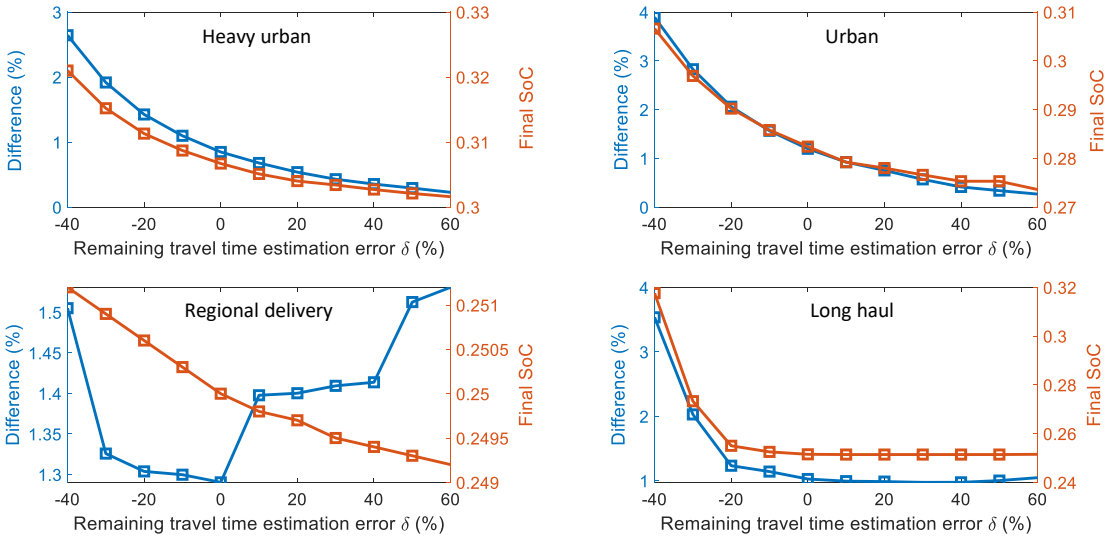

Fig. 13 Sensitivity study of inaccurate remaining travel time estimation on fuel economy

time per iteration of a model predictive controller can reach up to 10 seconds [25].

B. *Sensitivity analysis*

The proposed strategy adopts readily available navigation signals, such as the remaining distance and remaining time. The remaining distance normally can be well evaluated using a GPS based on a specified route. Nevertheless, the remaining time would be difficult to be accurately evaluated, due to the uncertainties of traffic. Hence it is worth analyzing the influences of inaccurate remaining travel time on fuel economy.

Supposing the estimated remaining time $\boldsymbol{t_{est}}$ is given by:

$$t_{est} = (1 + \delta) t_{est\_acurate} \tag{46}$$

where $t_{est\_acurate}$ is the accurate remaining time and δ is the estimation error of the navigation system.

In this study, an estimation error δ from -40% to 60% with a step of 10% along the whole driving cycle is analyzed. The different remaining time is applied to (43). The λ_{opt} strategy is used a benchmark to calculate the error, as shown in Fig. 13. As the estimation error δ varies from -40% to 0, there is an improvement in estimation accuracy. This improvement subsequently leads to the convergence of final SoC and fuel consumption towards the scenario where δ is 0. On the other hand, when the estimation error δ varies from 0 to 60%, it leads to an increase in the remaining travel time, causing a subsequent decrease in the average velocity for the remainder of the cycle. (see (43)). Consequently, the average force $\overline{F_{wh\_ref}}$ is decreased, as air resistance is proportional to the square of velocity (see (11)). This led to an increase in the rate of SoC, as shown in (37), resulting in a quicker depletion of the battery. As a result, the final SoC slightly decreased. Regarding the difference in fuel consumption compared to the benchmark, it is decreasing with the increase of δ under heavy urban, urban, and long haul. This phenomenon is reasonable because more electricity is used as the final SoC decreased. As for the regional delivery, the difference increased when δ is positive. This phenomenon is attributed to the system's nonlinear property. That is, the change in fuel consumption does not exhibit a straightforward positive correlation with the change in the rate of SoC. Instead, an increase in the SoC rate could lead to both an increase and a decrease in fuel consumption, depending on the specific conditions and factors involved.

In summary, the sensitivity study reveals that the fuel economy of the proposed strategy remains robust even with inaccurate navigation signals. When compared to accurate remaining time estimation, the maximal difference in fuel consumption with an estimation error ranging from -40% to 60% is less than 3% compared to the accurate scenario. This promising result indicates its potential applicability to existing vehicular control units without the need for additional hardware.

V. Conclusion

This paper presents an innovative state of charge planning method for a plug-in hybrid truck, which is based on verified high-level truck models. The modeling and control of the truck are organized in a forward approach using the energetic macroscopic representation. To test the adaptiveness of the strategy, four random driving cycles representing two vocational uses are employed. Furthermore, the sensitivity of inaccurate navigation signals on fuel economy is analyzed.

The proposed strategy only requires the target distance, traveled distance, and remaining travel time. These signals are readily available from the navigation system, making it possible to implement the strategy on an existing vehicular control unit without the need for additional hardware. By utilizing instant navigation signals, the strategy can adapt to variations in traffic conditions and environments. Simulation results demonstrate that, in comparison to the optimal strategy for unknown urban and long-haul delivery cycles, the proposed strategy only increases fuel consumption by a maximum of 1.3%. A sensitivity study reveals the robustness of the method on inaccurate navigation signals. This indicates that the proposed method is highly efficient, adaptive, and cost-effective for real-time truck applications. Furthermore, the method can be extended to other types of plug-in hybrid electric vehicles, such as plug-in passenger cars.

ACKNOWLEDGEMENT

This work has been achieved within the frame of the CE2I (Intelligent Integrated Energy Converter) and EE40 (Electrical Energy 4.0) projects. CE2I and EE4.0 are co-financed by European Union with the financial support of the European Regional Development Fund (ERDF), the French state, and the French Region of Hauts-de-France.

REFERENCES

[1] F. Rodríguez, "Fuel consumption simulation of HDVs in the EU: Comparisons and limitations," *ICCT White Pap*, 2018.

[2] B. Müller, C. Zachäus, and G. Meyer, "European strategic processes towards competitive, sustainable and user-friendly electrified road transport," in *30th international electric vehicle symposium, Stuttgart*, 2017, vol. 10.

[3] D. Smith *et al.*, "Medium-and heavy-duty vehicle electrification: An assessment of technology and knowledge gaps," Oak Ridge National Lab.(ORNL), Oak Ridge, TN (United States), 2020.

[4] Y. Li, X. Deng, B. Liu, J. Ma, F. Yang, and M. Ouyang, "Energy management of a parallel hybrid electric vehicle based on Lyapunov algorithm," *eTransportation*, vol. 13, p. 100184, 2022.

[5] S. Xie, X. Hu, T. Liu, S. Qi, K. Lang, and H. Li, "Predictive vehicle-following power management for plug-in hybrid electric vehicles," *Energy*, vol. 166, pp. 701-714, 2019.

[6] S. Cordiner, M. Galeotti, V. Mulone, M. Nobile, and V. Rocco, "Trip-based SOC management for a plugin hybrid electric vehicle," *Applied Energy*, vol. 164, pp. 891-905, 2016.

[7] X. Lin, Y. Xia, W. Huang, and H. Li, "Trip distance adaptive power prediction control strategy optimization for a Plug-in Fuel Cell Electric Vehicle," *Energy*, vol. 224, p. 120232, 2021.

[8] X. Lin, X. Xu, and H. Lin, "Predictive-ECMS based degradation protective control strategy for a fuel cell hybrid electric vehicle considering uphill condition," *ETransportation*, vol. 12, p. 100168, 2022.

[9] Y. Du, Y. Zhao, Q. Wang, Y. Zhang, and H. Xia, "Trip-oriented stochastic optimal energy management strategy for plug-in hybrid electric bus," *Energy*, vol. 115, pp. 1259-1271, 2016.

[10] Z. Lei, D. Qin, L. Hou, J. Peng, Y. Liu, and Z. Chen, "An adaptive equivalent consumption minimization strategy for plug-in hybrid electric vehicles based on traffic information," *Energy*, vol. 190, p. 116409, 2020.

[11] B.-H. Nguyen, R. German, J. P. F. Trovão, and A. Bouscayrol, "Real-time energy management of battery/supercapacitor electric vehicles based on an adaptation of Pontryagin's minimum principle," *IEEE transactions on Vehicular Technology*, vol. 68, no. 1, pp. 203-212, 2018.

[12] J. Li, Y. Liu, D. Qin, G. Li, and Z. Chen, "Research on equivalent factor boundary of equivalent consumption minimization strategy for PHEVs," *IEEE Transactions on Vehicular Technology*, vol. 69, no. 6, pp. 6011-6024, 2020.

[13] A. Rezaei, J. B. Burl, and B. Zhou, "Estimation of the ECMS equivalent factor bounds for hybrid electric vehicles," *IEEE Transactions on Control Systems Technology*, vol. 26, no. 6, pp. 2198-2205, 2017.

[14] K. Deng *et al.*, "An adaptive PMP-based model predictive energy management strategy for fuel cell hybrid railway vehicles," *ETransportation*, vol. 7, p. 100094, 2021.

[15] C. Sun, F. Sun, X. Hu, J. K. Hedrick, and S. Moura, "Integrating traffic velocity data into predictive energy management of plug-in hybrid electric vehicles," in *2015 American control conference (ACC)*, 2015: IEEE, pp. 3267-3272.

[16] S. Zhang and R. Xiong, "Adaptive energy management of a plug-in hybrid electric vehicle based on driving pattern recognition and dynamic programming," *Applied Energy*, vol. 155, pp. 68-78, 2015.

[17] Y. Zhou, A. Ravey, and M.-C. Péra, "Multi-objective energy management for fuel cell electric vehicles using online-learning enhanced Markov speed predictor," *Energy Conversion and Management*, vol. 213, p. 112821, 2020.

[18] Y. Du, N. Cui, W. Cui, Z. Chen, and C. Zhang, "Receding horizon control based energy management strategy for PHEB using GRU deep learning predictive model," *eTransportation*, vol. 13, p. 100179, 2022.

[19] H. Tan, H. Zhang, J. Peng, Z. Jiang, and Y. Wu, "Energy management of hybrid electric bus based on deep reinforcement learning in continuous state and action space," *Energy Conversion and Management*, vol. 195, pp. 548-560, 2019.

[20] S. Zendegan, A. Ferrara, S. Jakubek, and C. Hametner, "Predictive battery state of charge reference generation using basic route information for optimal energy management of heavy-duty fuel cell vehicles," *IEEE Transactions on Vehicular Technology*, vol. 70, no. 12, pp. 12517-12528, 2021.

[21] S. Xie, X. Hu, Z. Xin, and J. Brighton, "Pontryagin's minimum principle based model predictive control of energy management for a plug-in hybrid electric bus," *Applied energy*, vol. 236, pp. 893-905, 2019.

[22] X. Lin, J. Wu, and Y. Wei, "An ensemble learning velocity prediction-based energy management strategy for a plug-in hybrid electric vehicle considering driving pattern adaptive reference SOC," *Energy*, vol. 234, p. 121308, 2021.

[23] H.-Q. Guo, G. Wei, F. Wang, C. Wang, and S. Du, "Self-learning enhanced energy management for plug-in hybrid electric bus with a target preview based SOC plan method," *IEEE Access*, vol. 7, pp. 103153-103166, 2019.

[24] H. Zhang, J. Peng, H. Tan, H. Dong, F. Ding, and B. Ran, "Tackling SOC long-term dynamic for energy management of hybrid electric buses via adaptive policy optimization," *Applied energy*, vol. 269, p. 115031, 2020.

[25] M. R. Amini, I. Kolmanovsky, and J. Sun, "Hierarchical MPC for robust eco-cooling of connected and automated vehicles and its application to electric vehicle battery thermal management," *IEEE Transactions on Control Systems Technology*, vol. 29, no. 1, pp. 316-328, 2020.

[26] M. Josevski and D. Abel, "Energy management of parallel hybrid electric vehicles based on stochastic model predictive control," *IFAC Proceedings Volumes*, vol. 47, no. 3, pp. 2132-2137, 2014.

[27] L. Li, S. You, C. Yang, B. Yan, J. Song, and Z. Chen, "Driving-behavior-aware stochastic model predictive control for plug-in hybrid electric buses," *Applied Energy*, vol. 162, pp. 868-879, 2016.

[28] W. Zhou, Y. Chen, H. Zhai, and W. Zhang, "Predictive energy management for a plug-in hybrid electric vehicle using driving profile segmentation and energy-based analytical SoC planning," *Energy*, vol. 220, p. 119700, 2021.

[29] W. Zhou, X. Cai, Y. Chen, J. Li, and X. Peng, "Decoding the optimal charge depletion behavior in energy domain for predictive energy management of series plug-in hybrid electric vehicle," *Applied Energy*, vol. 316, p. 119098, 2022.

[30] J. Shangguan, H. Guo, and M. Yue, "Robust energy management of plug-in hybrid electric bus considering the uncertainties of driving cycles and vehicle mass," *Energy*, vol. 203, p. 117836, 2020.

[31] F. Rodríguez and O. Delgado, "The Future of VECTO: CO_2 Certification of Advanced Heavy-Duty Vehicles in the European Union," 2019.

[32] A. Bouscayrol, J. P. Hautier, and B. Lemaire-Semail, "Graphic formalisms for the control of multi-physical energetic systems: COG and EMR," *Systemic design methodologies for electrical energy systems: analysis, synthesis and management*, pp. 89-124, 2012.

[33] R. Tomas, G. Martirano, and H. Matthew, "The European Commission's science and knowledge service," 2019.

[34] A. Pam, A. Bouscayrol, P. Fiani, and F. Faval, "Comparison of different models for energy management strategy design of a parallel hybrid electric vehicle: Impact of the rotating masses," *IET Electrical Systems in Transportation*, vol. 11, no. 1, pp. 36-46, 2021.

[35] M. R. KGaA, "Der Reifen: Rollwiderstand Und Kraftstoffersparnis," *Clermont-Ferrand, France*, 2005.

[36] L. Boulon, A. Bouscayrol, D. Hissel, O. Pape, and M.-C. Pera, "Inversion-based control of a highly redundant military HEV," *IEEE transactions on Vehicular Technology*, vol. 62, no. 2, pp. 500-510, 2012.

[37] A. Castaings, W. Lhomme, R. Trigui, and A. Bouscayrol, "Comparison of energy management strategies of a battery/supercapacitors system for electric vehicle under real-time constraints," *Applied Energy*, vol. 163, pp. 190-200, 2016.

[38] K. Li, A. Bouscayrol, S. Cui, and S. Han, "Energetic macroscopic representation and inversion-based control of an electrical vehicle using

modular cascade machines," in *2016 IEEE Vehicle Power and Propulsion Conference (VPPC)*, 2016: IEEE, pp. 1-6.
[39] W. Lhomme, A. Bouscayrol, S. A. Syed, S. Roy, F. Gailly, and O. Pape, "Energy savings of a hybrid truck using a ravigneaux gear train," *IEEE Transactions on Vehicular Technology*, vol. 66, no. 10, pp. 8682-8692, 2017.
[40] K. Li, W. Lhomme, and A. Bouscayrol, "Plug-in Hybridization of a Medium-Duty Truck Considering Total Cost of Ownership," in *2021 IEEE Vehicle Power and Propulsion Conference (VPPC)*, 2021: IEEE, pp. 1-6.
[41] N.-G. Zacharof and G. Fontaras, "Report on VECTO technology simulation capabilities and future outlook," *Publications Office of the European Union: Luxembourg*, 2016.
[42] Y. Y. Chia, L. H. Lee, N. Shafiabady, and D. Isa, "A load predictive energy management system for supercapacitor-battery hybrid energy storage system in solar application using the Support Vector Machine," *Applied Energy*, vol. 137, pp. 588-602, 2015.
[43] J. Cervantes, F. Garcia-Lamont, L. Rodríguez-Mazahua, and A. Lopez, "A comprehensive survey on support vector machine classification: Applications, challenges and trends," *Neurocomputing*, vol. 408, pp. 189-215, 2020.
[44] R. Schmid, J. Buerger, and N. Bajcinca, "Energy management strategy for plug-in-hybrid electric vehicles based on predictive PMP," *IEEE Transactions on Control Systems Technology*, vol. 29, no. 6, pp. 2548-2560, 2021.
[45] S. Xie *et al.*, "Model predictive energy management for plug-in hybrid electric vehicles considering optimal battery depth of discharge," *Energy*, vol. 173, pp. 667-678, 2019.
[46] C. Mayet *et al.*, "Comparison of different models and simulation approaches for the energetic study of a subway," *IEEE transactions on Vehicular Technology*, vol. 63, no. 2, pp. 556-565, 2013.